JOURNAL OF GEOPHYSICAL RESEARCH, VOL. 115, B03304, doi:10.1029/2009JB006689, 2010

Correlation of earthquake source parameters inferred from dynamic rupture simulations

Jan Schmedes,[1,2] Ralph J. Archuleta,[1,2] and Daniel Lavallée[1]

Received 11 June 2009; revised 8 October 2009; accepted 21 October 2009; published 6 March 2010.

[1] We analyzed 315 dynamic strike-slip rupture models computed up to 5.0 Hz to get a quantitative understanding of the correlation and amplitude distributions of parameters describing the earthquake source, such as slip and rupture velocity. To account for the epistemic uncertainty of the problem, we constructed a database of dynamic ruptures computed by ourselves and other authors. This database contains ruptures computed using different models of initial stress, peak stress, and critical slip-weakening distance. Using the set of computed ruptures, we constructed probability density functions (pdfs) for the amplitude distributions of the source parameters and for the correlation between the source parameters. We tried to extract parameter pairs that showed a small variability in the spatial correlation given the large epistemic uncertainty in the input. We only analyzed the areas on the fault with subshear propagation speed. The principal findings are as follows: (1) Final slip amplitude does not show correlation with the local rupture velocity. (2) Final slip amplitude correlates well with risetime. (3) Rupture velocity correlates well with peak slip rate and the duration of the impulsive part of the slip rate function. (4) The pdf of rupture velocity, risetime, and peak slip rate depends on the distance from the nucleation zone. (5) Fracture energy is not the single controlling factor for the rupture velocity; the slope of the linear slip-weakening curve has a significant effect on the rupture velocity. (6) The crack length (length that is slipping at a given time) decreases with the distance from the nucleation zone.

Citation: Schmedes, J., R. J. Archuleta, and D. Lavallée (2010), Correlation of earthquake source parameters inferred from dynamic rupture simulations, *J. Geophys. Res.*, *115*, B03304, doi:10.1029/2009JB006689.

1. Introduction

[2] Predicting seismic ground motion requires a full understanding of the physics of the earthquake process or at the very least, a reasonable approximation to the physics. Two approaches, kinematic and dynamic, are used to compute ground motion for a finite earthquake source. In both approaches, the fault surface is modeled as an internal boundary. In a kinematic model, a slip boundary condition is used where the full spatiotemporal evolution of slip is prescribed. The advantage of a kinematic description is that it can be computed efficiently for all frequencies. But it makes the strong assumption that we know the spatiotemporal evolution of slip during an earthquake. In a dynamic model the initial state of stress is given together with a friction law that describes how the shear stress evolves on the fault surface; that is, stress boundary conditions are used. A dynamic model computes the full spatiotemporal evolution of slip on the fault surface. But even if the physics were relatively well known, there are computational restrictions that limit the maximum frequency of the seismic ground motion that might be computed using a dynamic model. A workable compromise is to use a physics-based rupture model as input to a kinematic rupture for which the ground motion can be computed to higher frequencies. For instance, according to *Guatteri et al.* [2004, p. 2051], pseudo-dynamic models are kinematic source descriptions "designed to emulate important characteristics of dynamic rupture."

[3] The basis of such a pseudo-dynamic model is an understanding of the spatial interdependency of the earthquake source parameters, such as slip and rupture velocity. On the basis of the observation of a spatial correlation between kinematic source parameters, *Archuleta* [1984], *Oglesby and Day* [2002], and *Liu et al.* [2006] developed a model that describes the kinematic source parameters as spatially correlated random fields.

[4] To get a more quantitative understanding of the spatial correlation between earthquake source parameters and their amplitude distributions, dynamic modeling of the earthquake rupture process is necessary. To achieve robust statistics, many dynamic models have to be computed. Most ruptures analyzed in this study are computed using a slip-weakening friction law [*Ida*, 1972] shown in Figure 1. We also computed some ruptures using a time-weakening law [*Andrews*, 2004].

[5] Crucial for such computations is the choice of realistic initial stress and peak stress (also called strength in the

[1]Institute for Crustal Studies, University of California, Santa Barbara, California, USA.
[2]Department of Earth Science, University of California, Santa Barbara, California, USA.

0148-0227/10/2009JB006689$09.00

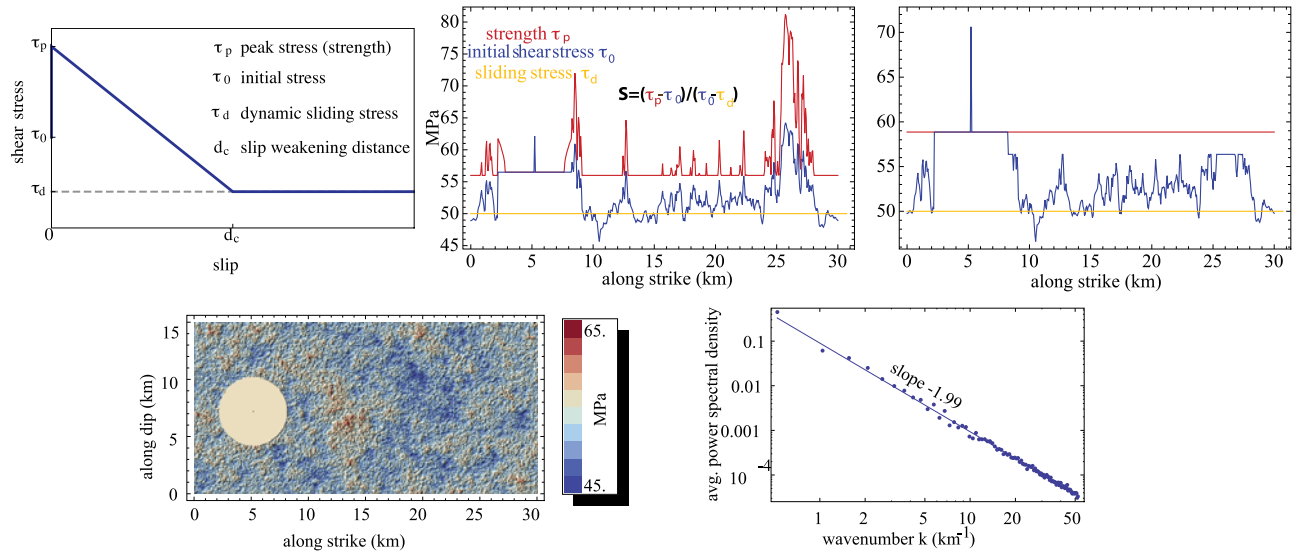

Figure 1. (top) Linear slip. (left) Linear slip-weakening friction law. Along-strike profiles of sliding stress, initial shear stress, and strength computed using (middle) constant S factor or (right) constant strength. The profiles are through the middle of the fault, more precisely, through the point at which the perturbation in initial stress is applied that triggers the spontaneous rupture (blue peak in constant region at about 5 km along strike). (bottom) Example. (left) Example of initial shear stress field with power spectral decay of 2 projected on the fault plane. The circle with constant initial shear stress is the nucleation region. (right) Average power spectral density. The blue points are computed by averaging the power spectrum of the initial shear stress field along circles with constant k. The line is fitted through the points.

following). Several models have been proposed in the literature to describe the spatial correlation, or the power spectrum, associated with the slip or the stress spatial variability [e.g., *Lavallée et al.*, 2006; *Mai and Beroza*, 2002]. In these models, the power spectrum is asymptotically attenuated according to a power law with exponent ν [*Lavallée et al.*, 2006; *Lavallée*, 2008]. For the strength distribution there is no direct guidance based on data; typical choices include using constant strength [*Ripperger et al.*, 2008] or a constant ratio of strength excess over stress drop [*Ma et al.*, 2008].

[6] Such lack of knowledge is commonly described as epistemic uncertainty. It captures everything that requires one to make a choice (e.g., what power spectrum for initial stress, what constitutive law), i.e., everything where there is no consensus among researchers. In principle, a better understanding of epistemic uncertainty is achieved by investigating the outputs of numerical simulations on the basis of the competing hypothesis. Epistemic uncertainty can be reduced by research (for example, if some of the competing hypothesis can be ruled out). Accounting for this epistemic uncertainty is very important because of bias and assumptions associated with one's favorite model. In this paper, initial models of stress and strength are based on various approaches commonly used in the literature. We implemented various approaches for a heterogeneous critical slip-weakening distance, such as constant fracture energy or a constant slope of the linear slip-weakening law over the whole rupture plane. In addition to the slip-weakening friction law, we also implemented the time-weakening friction law [*Andrews*, 2004] in several scenarios. For this friction law, we assumed that the breakdown time is constant, producing good resolution of the breakdown zone. In this type of friction law, the critical slip-weakening distance is also heterogeneous but determined dynamically. In addition, we also included dynamic ruptures computed by other researchers [*Dalguer et al.*, 2008; *Olsen et al.*, 2009]. We did this to account for the epistemic uncertainty and to avoid being biased by our choices. Furthermore, to account for natural variability, described as aleatoric uncertainty, we computed multiple random realizations for each approach.

[7] For each rupture, we computed the spatial correlation as a linear estimator of the spatial interdependency between different pairs of source parameters, for example, rupture velocity and slip amplitude. Using the spatial correlations of all rupture models, we then computed a probability density function (pdf) of the correlation for each pair of source parameters. Our goal in this study is to find parameter pairs that have a spatial interdependency that is common among all models. Such a parameter pair would have a modal and narrow pdf of spatial correlation. In short, we tried to find the set of parameters that shows the least variability in the spatial correlation coefficient for the given epistemic and aleatoric uncertainty present in our dynamic rupture catalog. To validate the procedure, we also looked at the joint distributions. Furthermore, we looked at some subsets of our catalog to see if our results are stable or if some systematic behavior can be observed.

[8] In addition, we looked at some scenarios in order to investigate factors that control the rupture velocity. Using a two-dimensional model, *Andrews* [1976a] found a relation between rupture velocity, stress drop, crack length, and fracture energy. On the basis of this model, *Guatteri et al.* [2004] adopted this finding to define a pseudo-dynamic model in which the rupture velocity is controlled by the

Table 1. Velocity Structures Used in This Study[a]

Structure	Thickness (km)	*P* Wave Velocity (km/s)	*S* Wave Velocity (km/s)	Density
Layer over half-space	5.4	4.33	2.5	2.7
Gradient over half-space	14.4	4.33 + z(0.866/14.4)	2.5 + z(0.5/14.4)	2.7 + z(0.3/14.4)
Half-space	-	5.196	3.0	3.0

[a]The layer and the gradient structure are both over a half-space. For the gradient structure, z is the variable for depth and runs between 0 km and 14.4 km.

fracture energy. Using a subset of ruptures, we tested if the fracture energy is the single controlling factor of the rupture velocity. Furthermore, we investigated the behavior of the crack length (length that is slipping at a given time) as the rupture propagates along the fault.

2. Dynamic Models

2.1. Ruptures Computed by the Authors

[9] We used a structured mesh finite element code with one point integration and absorbing boundaries to compute dynamic ruptures for a strike slip fault in a 3-D medium (see *Ma and Liu* [2006] for details). Because we had to compute a large number of ruptures, we used the message passing interface to parallelize the code. The friction on the fault plane is described by a linear slip-weakening [*Ida*, 1972] or linear time-weakening [*Andrews*, 2004] law. The total number of ruptures computed and analyzed is 315.

[10] All of the computed ruptures are pure strike slip on a vertical fault. The ruptures are either buried or break the surface. We computed ruptures for fault lengths between 30 and 120 km and rupture widths between 12 and 20 km in three different 1-D velocity structures: half-space, 1 layer over half-space, and 1-D velocity gradient (see Table 1).

[11] We used a grid spacing of h = 60 m in our computations, allowing us to analyze the ruptures up to 5.0 Hz (10 grid points per wavelength). We performed tests with smaller time steps dt and smaller grid spacing h to ensure that our results converged. We included five ruptures, which are computed using a grid spacing of 30 m, with a dimension 30 km × 15 km.

[12] We used a constant normal stress of 100 MPa in most models; 14 ruptures are computed using a depth-dependent normal stress and stress drop. The dynamic coefficient of friction is held constant at a value of 0.5 in all models.

[13] Initial shear stress is spatially heterogeneous on the fault. To compute the initial shear stress, we used an approach in which the power spectrum of initial shear stress is attenuated according to a power law with exponent ν [*Lavallée et al.*, 2006; *Lavallée*, 2008]. The power spectrum of the initial stress is proportional to $k^{-\nu}$, where k is the 2-D radial wave number. We used exponents ν = 1, 2, 3, and 4 (Figure 1 and Figure S1 in the auxiliary material).[1] As an alternative to this approach, we constructed slip maps using the method developed by *Liu et al.* [2006] and computed the stress drop using a relation discussed by *Andrews* [1980]. By adding a constant dynamic sliding stress, we determined the initial shear stress (Figure S2).

[14] The static coefficient of friction (peak stress if multiplied by the normal stress) is either constant (Figure 1) or spatially heterogeneous on the fault. When modeling a heterogeneous distribution, the S factor [*Andrews*, 1976b; *Das and Aki*, 1977] (equation (1)) either takes a constant value across the fault (Figure 1) or varies randomly over the fault:

$$S = \frac{\tau_p - \tau_0}{\tau_0 - \tau_d}. \quad (1)$$

The parameter τ_p corresponds to the peak stress (strength), τ_0 corresponds to the initial stress, and τ_d corresponds to the dynamic sliding stress (see Figure 1). In the following, we call $\tau_p - \tau_d$ strength drop and $\tau_p - \tau_0$ strength excess.

[15] To ensure the ruptures are causal and no triggering occurs ahead of the rupture front, we prescribed a minimal strength drop for the heterogeneous strength models or minimal strength excess for models with constant strength. Because we did not expect that parts of the fault had zero strength before an earthquake, using a finite positive value was reasonable. For a subset of ruptures we included restrengthening of the fault; that is, once a point stops rupturing, its strength is set back to the initial value.

[16] The critical slip-weakening distance is either constant or spatially heterogeneous on the fault. To construct a spatially heterogeneous distribution, we (1) constrained the fracture energy to be constant (correlation between strength and critical slip-weakening distance), (2) constrained the slope of the linear slip-weakening law to be constant (anti-correlation between strength and critical slip-weakening distance), (3) increased the slip-weakening distance linearly with the distance from the nucleation point, and (4) computed it dynamically by implementing time-weakening friction [*Andrews*, 2004]. This implementation is chosen for the longest ruptures to ensure the breakdown zone is well resolved for distances farther away from the hypocenter because in general, the breakdown zone is expected to shrink as the rupture propagates along the fault plane.

[17] We nucleated the ruptures by either setting a circular area of initial shear stress with a radius of 2.7 km above the strength or equal to the level at strength. In the second case, only the center point is elevated above the level of strength (Figure 1). This yields a slow nucleation that mimics a triggered rupture [*Campillo et al.*, 2001]. For the time-weakening model we set the critical time T_{dc} (time at which slip equals slip-weakening distance) at a value of 1.2 s inside the nucleation area to achieve slow nucleation and then linearly decreased it to 0.308 s (dt = 0.011 s) over a distance of 1.5 km.

2.2. Ruptures Computed by Other Researchers

[18] *Dalguer et al.* [2008] and *Olsen et al.* [2009] provided us with six 300 km long strike-slip ruptures that were computed in the 3-D velocity structure of southern California. They constructed their initial models using the slip-matching technique; they also used a linear slip-

[1]Auxiliary materials are available in the HTML. doi:10.1029/2009JB006689.

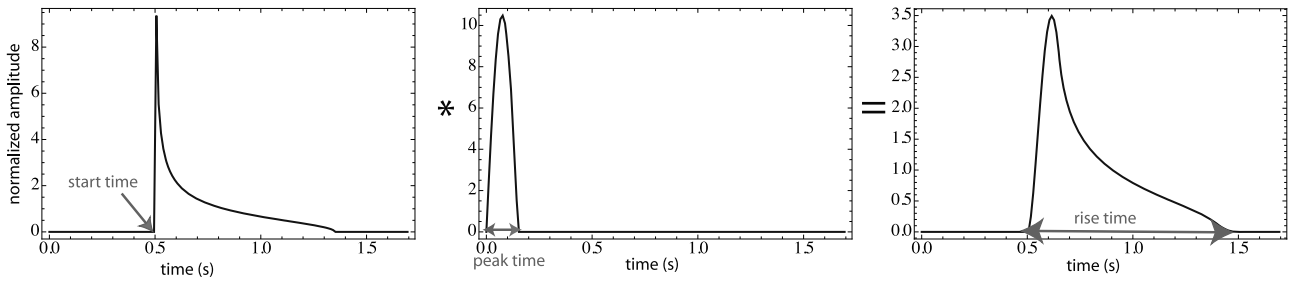

Figure 2. Illustration of slip rate function defined in equation (2). The start time corresponds to T_0, the peak time corresponds to T_p, and the risetime corresponds to T_r. The peak time controls the duration of the positive slip acceleration.

weakening friction law. They set the critical slip-weakening distance constant for most of the fault except for a layer on top that has a larger value to mimic velocity strengthening. They nucleated by setting a circular area above the level of strength and by lowering the critical slip-weakening distance inside that area.

3. Extraction of Kinematic Source Parameters

[19] We computed several kinematic parameters from the dynamic slip time history on the fault in order to analyze correlations among them. Because there is no restrengthening in the slip-weakening description for a large number of ruptures in the database, points on the fault can slip for a long time at low slip rates because of the lack of healing. In order to extract risetimes T_r relevant for kinematic modeling, we fitted a slip rate function $\dot{s}(t)$ that is constructed by convolving the slip rate function by *Nielsen and Madariaga* [2003] with a half sine of width T_p (R. Madariaga, personal communication, 2008) to the dynamically computed slip rate time series. This slip rate function is defined in equation (2) for $t \geq 0$ and is illustrated in Figure 2. The function $H(t)$ is the Heaviside function, and T_0 is the rupture time. The constant A is given by imposing the condition $\int_{-\infty}^{\infty} \dot{s}(t)\mathrm{d}t = 1$:

$$\dot{s}(t) = A\mathrm{Re}\left(\frac{\sqrt{T_0 + T_r - T_p - t}}{\sqrt{t - T_0}}\right) * H(T_p - t)\sin\left(\pi\frac{t}{T_p}\right). \quad (2)$$

Note that this formulation of the slip rate function is very similar to the formulation introduced by *Tinti et al.* [2005] and used by *Tinti et al.* [2009]. In their studies, they use a triangle instead of a half sine. They show that the half-length of the triangular function, the equivalent of our parameter T_p, is linearly related to the time to reach the peak slip velocity (i.e., duration of positive slip acceleration). Hence, the peak time T_p controls the duration of the impulsive part of the slip rate function.

[20] For each point on the fault (about 60 million total for all ruptures combined), we fitted the described slip rate function by minimizing a least squares cost function with the two parameters (T_0, T_p), using the downhill simplex method [*Nelder and Mead*, 1965; *Press et al.*, 1992]. In our procedure we only fitted the slip rate function to the part of the computed slip rate function until the time T_{end} at which the slip rate reaches zero for the first time (we did not account for the low-velocity sliding in our slip rate function; Figure 3). We normalized the dynamically computed slip rate function between zero and T_{end} before we performed the fitting. We computed the risetime as $T_r = T_{\mathrm{end}} - T_0$. From the dynamically computed slip rate (not normalized), we extracted the peak slip rate $\dot{s}_{\mathrm{max}}$ and the final slip s_{total}. Because points on the fault can slip for a long time at low rates, we computed a slip s_{kin} that is accumulated slip until the slip rate reaches zero for the first time, that is, the slip accumulated until time $T_0 + T_r$ (Figure 3).

[21] The dynamically computed slip rate functions show small-scale oscillations around the fitted slip rate function (see Figure 3), but overall, we found a good fit using the slip rate function given in equation (2). We also experimented with the slip rate function defined by *Liu et al.* [2006] but found a better fit for the slip rate function used in this study.

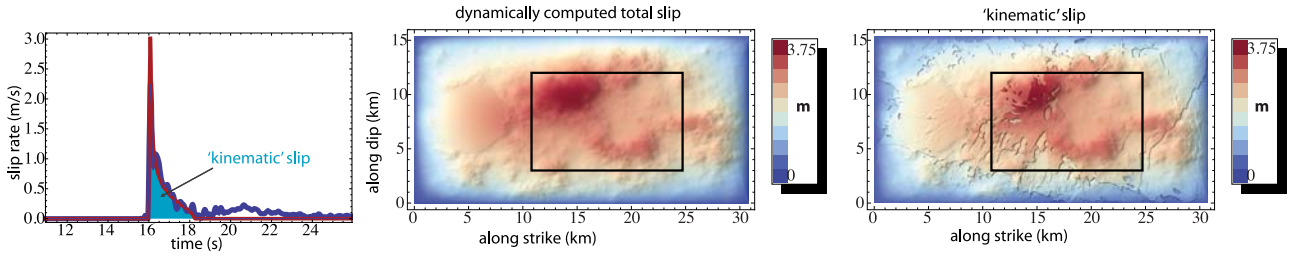

Figure 3. (left) Dynamically computed slip rate (blue) and fitted slip rate function (red). After the rupture stopped for the first time, there is no strength, and small perturbations can trigger low velocity sliding. The area under the curve from the start to the first stop of the rupture corresponds to (right) the kinematic slip. (middle) The total slip is the total slip at the end of the rupture. The black rectangles in Figures 3 (middle) and 3 (right) outline the area for which the statistical analysis is performed. The area does not include the nucleation region or the boundaries.

[22] We computed the local rupture velocity v_r as the inverse of the norm of the numerical gradient of the rupture time [*Oglesby and Day*, 2002]. In order to get a smooth rupture velocity distribution, we smoothed the two directional derivatives using a mask with a dimension of 240 m × 240 m before we computed the inverse norm of the numerical gradient. The weights of the mask are chosen according to a Gaussian function [see, e.g., *Gonzalez and Woods*, 2002] with a standard deviation of 60 m. In the following, we referred to the center of Gaussian mask, which has the largest weight, as point even though it contains contributions from an area with a dimension of 240 m × 240 m. The variable we used in our statistical analysis is not the rupture velocity itself but the ratio γ of rupture velocity v_r to the local shear wave velocity v_S. We also call this ratio normalized rupture velocity in the following. When the region surrounding the fault is a heterogeneous velocity structure, using the normalized rupture velocity reduces the variability of the pdf compared to using the local rupture velocity. In addition, it enabled us to create a probability density distribution using rupture models computed in different velocity structures. Finally, we also computed the secant velocity v_{sec} [*Day*, 1982], i.e., the average rupture velocity between the hypocenter and each point on the fault, as used by *Liu et al.* [2006].

4. Analysis of Kinematic Parameters

4.1. Spatial Interdependency

[23] To minimize the contribution of boundary or nucleation effects on our results, we selected only a part of the fault for our analysis; this part is the rectangular area outlined in Figures 3 and S3, which shows one example rupture. We are interested in correlation and amplitude distributions during the propagation of the rupture, not at nucleation or arrest. There is one additional constraint: within the rectangular area, we used only points on the fault that propagated at subshear speed.

[24] Because it is important that the breakdown zone is well resolved (at least five grid points), we approximated the breakdown distance for each point using the following approach: besides the rupture time T_0, we also computed the time T_{dc} at which the slip reaches the critical slip-weakening distance. Then, for each point on the fault x_{ij} we found the point y_{ij} on the fault that is closest in space and minimizes $|T_{dc}(y_{ij}) - T_0(x_{ij})|$. This point y_{ij} has reached the critical slip-weakening distance at about the same time at which the point x_{ij} starts slipping. Hence, y_{ij} is at the end of the breakdown zone of x_{ij}. We defined the distance between the two points as the breakdown distance. While this is an approximation, it is useful in identifying areas of the fault that are potentially not well resolved. In our analysis of spatial interdependency we excluded all points that had a breakdown distance less than five grid lengths (300 m). The largest fraction of the fault that potentially is not well resolved for our ruptures is 2%. To ascertain the effect of this 2%, we did tests with smaller grid spacing and with interpolated initial conditions. The tests showed stable results. Hence, this small fraction of the fault that has potentially fewer than five grid points inside the breakdown zone did not influence our results.

[25] By substituting the time T_{end} the rupture stops slipping for the time T_{dc} in the procedure for estimating the breakdown zone, we can approximate the crack length L using the same approach. While this is an approximation, it is useful to get an estimate of the range of crack lengths and how crack length depends on the length of the fault. This is discussed in more detail in section 4.5.

[26] For the points within the rectangle that propagate at subshear speed and have a well-resolved breakdown time, we computed the covariance matrix for zero lag (no offset between parameters) for the parameter vector (s_{total}, s_{kin}, T_p, T_r, γ, v_{sec}, $\dot{s}_{\max}$, $\tau_p - \tau_d$, $\tau_0 - \tau_d$). Using the variances and covariances, we can compute the correlation matrix as measure of linear spatial interdependency for all variables. Figure 4 shows the pdf for different parameter pairs (off-diagonal elements of the correlation matrix) for all rupture models.

[27] The first important result is contained in Figure 4 (top): the correlation of the slip s_{kin} with γ (ratio of rupture velocity to shear wave velocity). The distribution is centered on zero; hence, for most ruptures there is no correlation between these two parameters. Therefore, for a given slip distribution on the fault there are many different spatial distributions of γ possible, which translates into large variability in the possible ground motion. This result argues against using slip as a controlling parameter for rupture velocity [e.g., *Liu et al.*, 2006]. If a positive correlation between slip and rupture velocity is assumed, areas of large slip are sampled in a shorter time (faster rupture). This yields strong peaks in the ground motion because elastic waves radiated from the area of large slip arrive in a shorter time. Hence, if such a correlation is used, one might overpredict ground motion.

[28] However, slip does show a positive correlation with the risetime T_r; that is, larger slip is obtained for longer risetimes. Furthermore, T_r correlates positive with T_p (the parameter controlling the duration of the impulsive part of the slip rate function). Thus, points that have a long risetime have a less impulsive slip rate function.

[29] There is a positive correlation between the parameter γ and the peak slip rate and a negative correlation between γ and the peak time; that is, fast rupture velocities and short peak times accompany larger peak slip rate. The negative correlation between peak slip rate and peak time is also consistent with this picture. This interdependency of rupture velocity, peak slip rate, and peak time indicates that the rupture velocity is controlled during the weakening phase of the rupture, i.e., while the slip is smaller than the critical slip-weakening distance. This is consistent with the finding by *Andrews* [1976a], who predicted that the rupture velocity is related to the fracture energy. In addition to the fracture energy, the slope of the linear slip-weakening curve is important in controlling the rupture velocity, as discussed in section 4.4. A plot of the pdf of correlation for other parameter pairs is included and discussed in the auxiliary material (Figure S4). We observed the same qualitative behavior for total slip as for the kinematic slip. The secant velocity, which is used in the kinematic model by *Liu et al.* [2006], does not show consistent correlation with total slip; that is, there is a great variation in the observed correlations.

[30] Because correlation describes a linear relationship between two parameters, it is important to look at joint probabilities between the parameter pairs to better understand the results. For example, a parameter pair might show zero correlation but still be nonlinearly related. Also, outliers

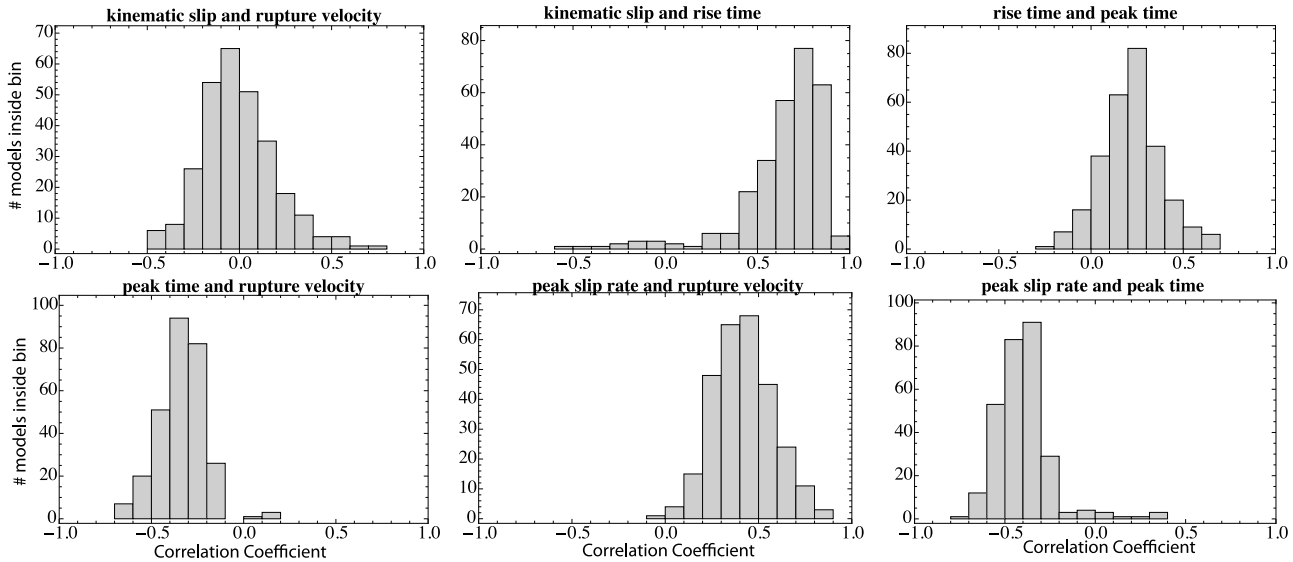

Figure 4. Histograms of computed spatial correlation coefficients for 315 ruptures and different parameter pairs. There is no correlation between slip and rupture velocity. Slip correlates positive with risetime, and risetime correlates positive with peak time. The rupture velocity correlates positive with peak slip rate and negative with peak time. Finally, the peak time correlates negative with peak slip rate.

can affect the computation of correlation (see Figure S5 for an example with artificial data). Figure 5 plots the joint distribution of slip divided by average slip and γ; it also plots the joint distribution for slip divided by average slip and risetime. The joint distribution was computed using all rupture models, but we randomly selected only 4000 fault points for each rupture (to keep the amount of data manageable). The plot for slip and normalized rupture velocity shows that once the rupture has accelerated to a fast speed, it is independent of the total slip. In fact, this is true for any rupture speed. In contrast, there is a clear positive relation between slip and risetime, as captured in the correlation of about 50% (here computed for all ruptures together). A similar plot for the subset of ruptures computed in the 3-D

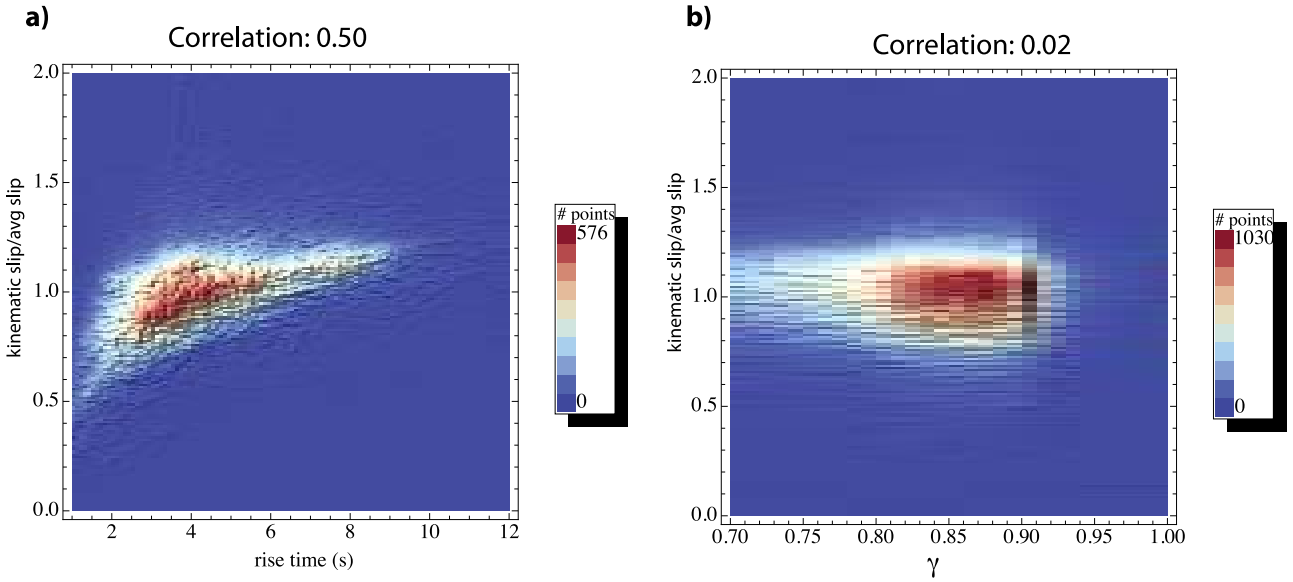

Figure 5. Joint distributions computed using 4000 points randomly selected from each rupture. (a) The spatial relation of slip divided by the average slip of a given event (necessary to plot all magnitudes together) and risetime. A clear positive trend can be found that is reflected in the computed correlation of 0.5. (b) The relation of slip divided by the average slip of a given event and normalized rupture velocity. There is no change of behavior for large or low slip; that is, there are as many points that rupture fast for low-slip regions as there are for high-slip regions. This is reflected in the very small correlation, which can be interpreted as zero correlation.

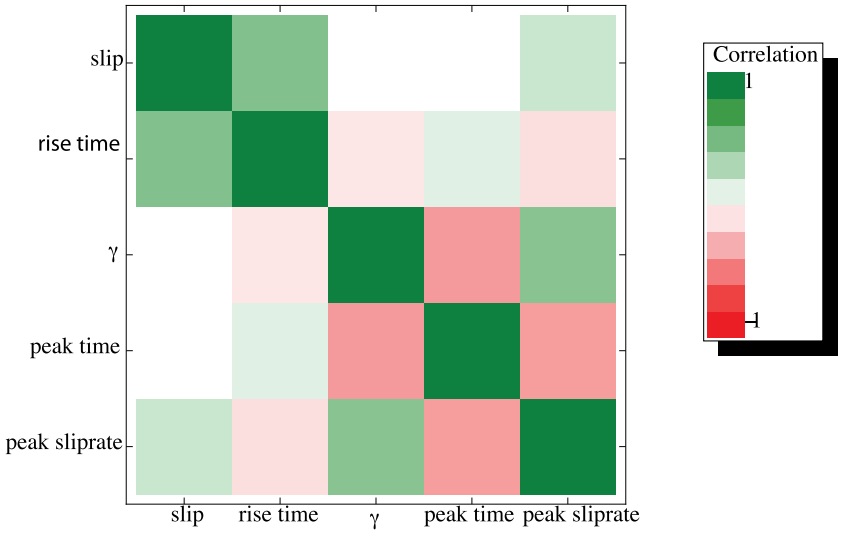

Figure 6. Correlation matrix computed 4000 randomly selected points from each dynamic model. Two regions of strong correlation are visible at top left between slip and risetime and at bottom right between rupture velocity over shear wave velocity, peak time, and peak slip rate.

velocity model of California [*Dalguer et al.*, 2008; *Olsen et al.*, 2009] is shown in the auxiliary material (Figure S6). There is a correlation of 0.27 for slip divided by average slip and rupture velocity divided by shear wave velocity. However, the joint distribution nicely illustrates that there is no simple linear relationship between the two. We found that the joint distribution had to be computed to understand the nature of the correlation (see also Figure S5).

[31] Instead of computing one correlation matrix for each rupture, we also computed a correlation matrix for all ruptures combined (using again 4000 randomly selected points for each rupture). The matrix for the parameters (s_{kin}, T_r, γ, T_p, $\dot{s}_{\mathrm{max}}$) is shown in Figure 6. The maximum correlation (off-diagonal) is found for slip and risetime, peak time and normalized rupture velocity, peak time and peak slip rate, and peak slip rate normalized rupture velocity. These were the same correlations we found when we examined the ensembles of individual ruptures.

[32] To test if our main results are stable, we compared the correlations for different subsets (Figure S7) and found no significant deviations. It is important to notice that our finding applies to the ensemble of scenarios and not necessarily to a single rupture. For instance, one may find a correlation between slip and rupture velocity for a given rupture. However, such correlation might be a coincidence (for example, low slip close to hypocenter and high slip at end of fault can yield positive correlation because the rupture accelerates along the fault; see section 4.2), or the correlation only exists for a certain type of initial conditions. Generalizing results on the basis of a single event or a small set of events can be misleading.

4.2. Amplitude Distributions

[33] Figure 7 shows the probability density functions for γ, risetime, and peak time. We computed the pdf using 4000 randomly selected points at which the rupture propagates at subshear speed for each rupture in our database. The normalized rupture velocity shows a strong mode at about 85% consistent with values found in the literature [*Somerville et al.*, 1999].

[34] Figure S8 plots the pdf for different subsets (for example, different length or different initial stress) of ruptures. Because ruptures with different lengths showed different distributions, we asked if there was a distance dependence for the amplitude distributions of the computed ruptures. We computed the pdfs as a function of distance from the nucleation zone for the six 120 km long ruptures in our database. We computed a pdf for each distance bin that

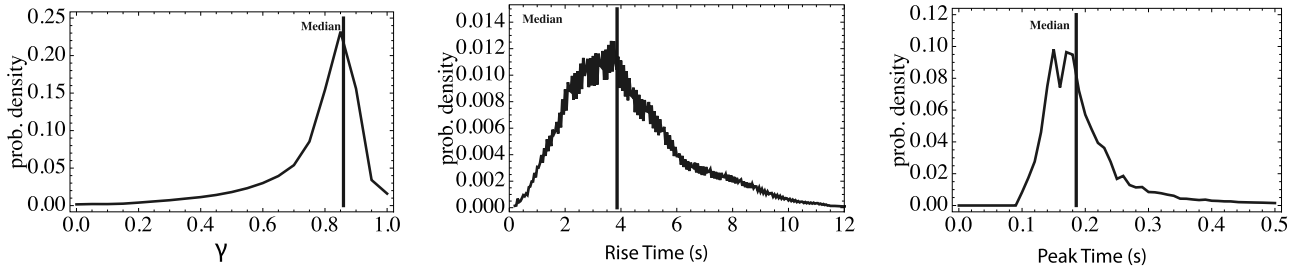

Figure 7. Probability density function for various earthquake source parameters computed using 4000 randomly selected points for each dynamic rupture model. Vertical lines show the median of each distribution.

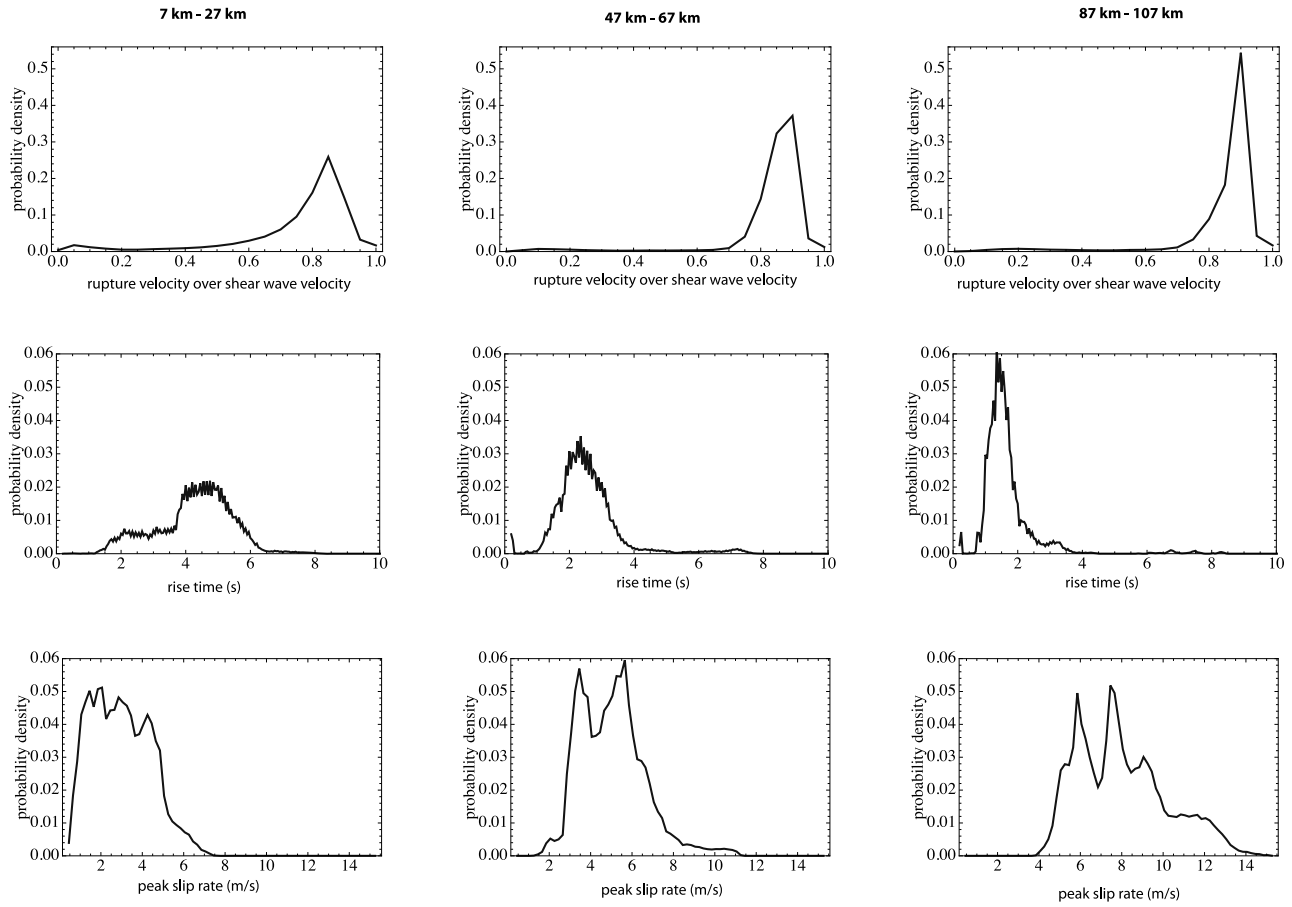

Figure 8. Probability density of various source parameters computed using different distance from the nucleation zone bins (20 km wide). Six 120 km long ruptures are used to compute the probability densities. One can clearly see a dependency on the distance to the nucleation zone.

has a length of 20 km, e.g., for all points that have distances from the center of the nucleation zone of 7–27 km, 27–47 km, etc. The length was chosen to achieve robust statistics. Figure 8 shows that the rupture accelerates with distance from the nucleation zone. Consequently, as predicted by the correlation shown in Figure 4, the peak slip rates increase as a function of distance. Likewise, the risetime gets shorter as the rupture travels along the fault. This distance dependence is another feature of dynamic models that should be accounted for in a kinematic description of a rupture.

4.3. Two-Dimensional Spatial Correlation

[35] All results discussed so far are for zero lag correlations. *Song et al.* [2009] propose looking at correlations for nonzero offset. For example, there might a fast rupture ahead of areas of large slip. To test this, we computed the 2-D coherence by selecting a smaller rectangle than the one previously used and then computed the correlation for each possible translation of this smaller rectangle inside the larger rectangle. We considered only ruptures larger than 60 km to ensure a sufficient number of samples to obtain robust statistics. For each translation, we computed the correlation for the points that propagated slower than the shear wave speed.

[36] Figure 9 plots the 2-D coherence maps computed by averaging the maps from 12 ruptures that are either 60 km or 120 km long. All the ruptures were computed using a time-weakening friction law, which ensures good resolution of the breakdown zone. We confirmed that these results also hold for ruptures computed using the slip-weakening law. We did not find any significant correlation between slip and rupture velocity for any translation, while risetime and slip correlate strongest at zero offset (no translation).

[37] The fact that there is no correlation between slip and rupture velocity for a given offset is also supported by theoretical findings. *Eshelby* [1969] showed that the rupture front can react instantaneously to changes in local conditions. This would counter the notion of a delayed reaction of the rupture front to previous conditions.

[38] An important feature in this study is that we limited our analysis to the areas of the fault that ruptured at subshear speed. If supershear was included, the situation would become much more complex. Stable supershear propagation can be caused by a rupture entering a region of high prestress or low strength (hence, low prestress) [*Liu and Lapusta*, 2008; *Schmedes et al.*, 2009]. In the first case, the transition to supershear occurs in regions of high slip; in the second case, the transition occurs in regions of low slip. If slip was interpreted as a control variable for the rupture front behavior, these situations would lead to conclusions that are opposite to each other. By looking at single events, one can always find

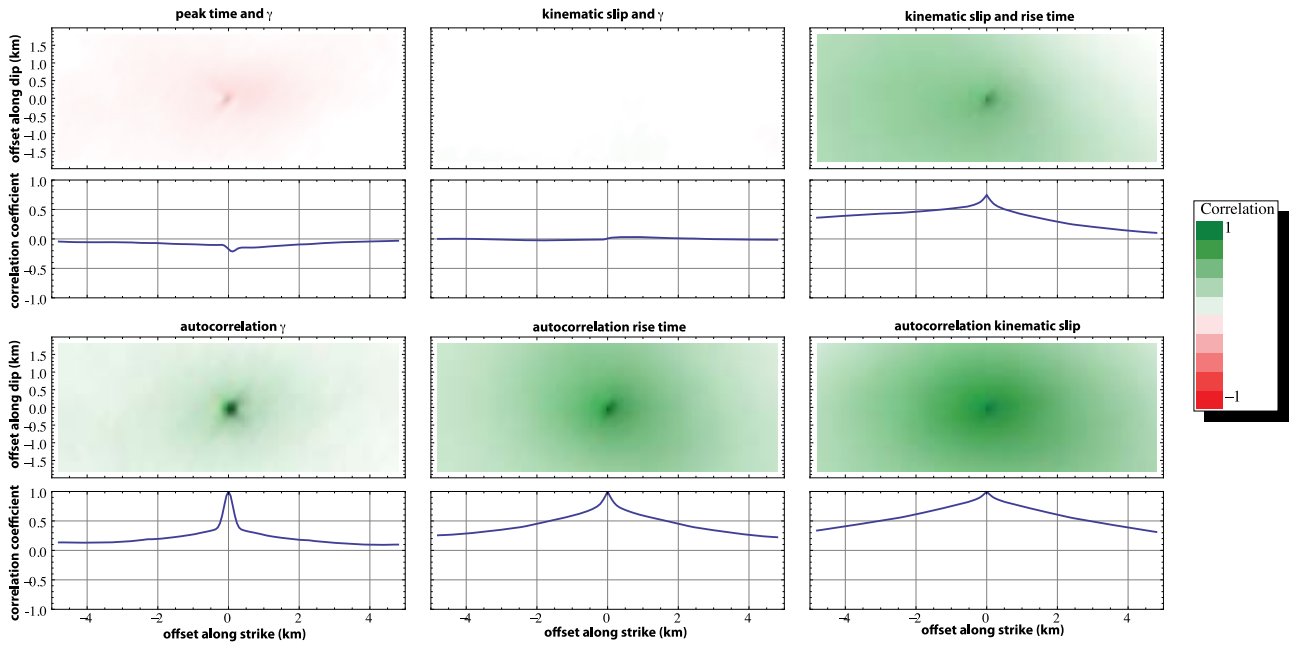

Figure 9. (top) Two-dimensional spatial coherence maps for cross correlation and (bottom) autocorrelation of various source parameters. One-dimensional plots show along-strike profile for zero offset along dip. Slip and rupture velocity do not show correlation for any offset. Slip and risetime show largest positive correlation at zero offset, while peak time and rupture velocity show the strongest negative correlation at zero offset.

cases where there is a zero offset correlation but they might not be physically meaningful.

[39] One important result that comes out from the analysis proposed by *Song et al.* [2009] is the distance at which the correlation drops below some threshold, i.e., how the correlation decays with distance. This decay is shown in Figure 9 (bottom). While rupture velocity correlates only over small offsets, slip and risetime show a slow decay of correlation with offset.

4.4. Fracture Energy

[40] In the model discussed by *Guatteri et al.* [2004] the fracture energy is used to control the rupture velocity [*Andrews*, 1976a]. To test the validity of this hypothesis, we selected six ruptures from our database that had a constant critical slip-weakening distance (referred to as set 1) and recomputed each using different amplitudes of stress, strength, and critical slip-weakening distance. To get a set 2, we kept the spatial heterogeneity of stress and strength but decreased the fracture energy of each point to two thirds of its original value (same S factor but smaller stress drop, strength excess, and critical slip-weakening distance). Alternatively, for set 3, we lowered strength excess and stress drop (S factor stays the same) but kept the critical slip-weakening distance at its original value. The different sets are illustrated in Figure 10 (top).

[41] Interestingly, even though set 2 has only two thirds of the total fracture energy in set 1, it has exactly the same rupture velocity and peak time distribution (Figure 10, bottom). Furthermore, both set 3 and set 1 have larger fracture energy than set 2, but set 3 has smaller rupture velocities than set 2, while set 1 has the same rupture velocities as set 2. These results suggest that in addition to the fracture energy, the slope of the slip-weakening curve significantly influences the rupture velocity.

[42] The peak slip rate gets larger for larger stress and strength drops. But if the stress and strength drops are the same, the slope of the slip-weakening curve controls the peak slip rate. While the peak slip rate gets larger for larger strength drops, the rupture velocity does not seem to depend on the absolute value of strength drop (as well as fracture energy) if the slope of the slip-weakening curve is the same. This slope controls the acceleration phase and, thus, influences the peak slip rate and the peak time. Both of those parameters correlate with the rupture velocity, which is also influenced by this slope.

4.5. Crack Length

[43] As described in section 4.1, we can approximate the crack length using the local time at which each point starts and stops rupturing. We used the 120 km long ruptures of our database that are computed using the time-weakening law [*Andrews*, 2004]. However, the following results are also valid for the other ruptures in our database.

[44] The important result from this analysis is that the crack length in heterogeneous 3-D models is limited. The crack length does not continuously grow as the rupture propagates along the fault, as in 2-D models [*Andrews*, 1976a]. Figure 11 shows the probability density for crack length as a function of distance from the hypocenter (similar to Figure 8). Our models show a behavior of the crack length similar to the length of the breakdown zone. As the rupture propagates away from the hypocenter, the crack length gets shorter. Compared to Figure 8, this shortening of the crack correlates with an acceleration of the rupture front and larger peak slip rates. In the 2-D case, the rupture gets faster as the crack

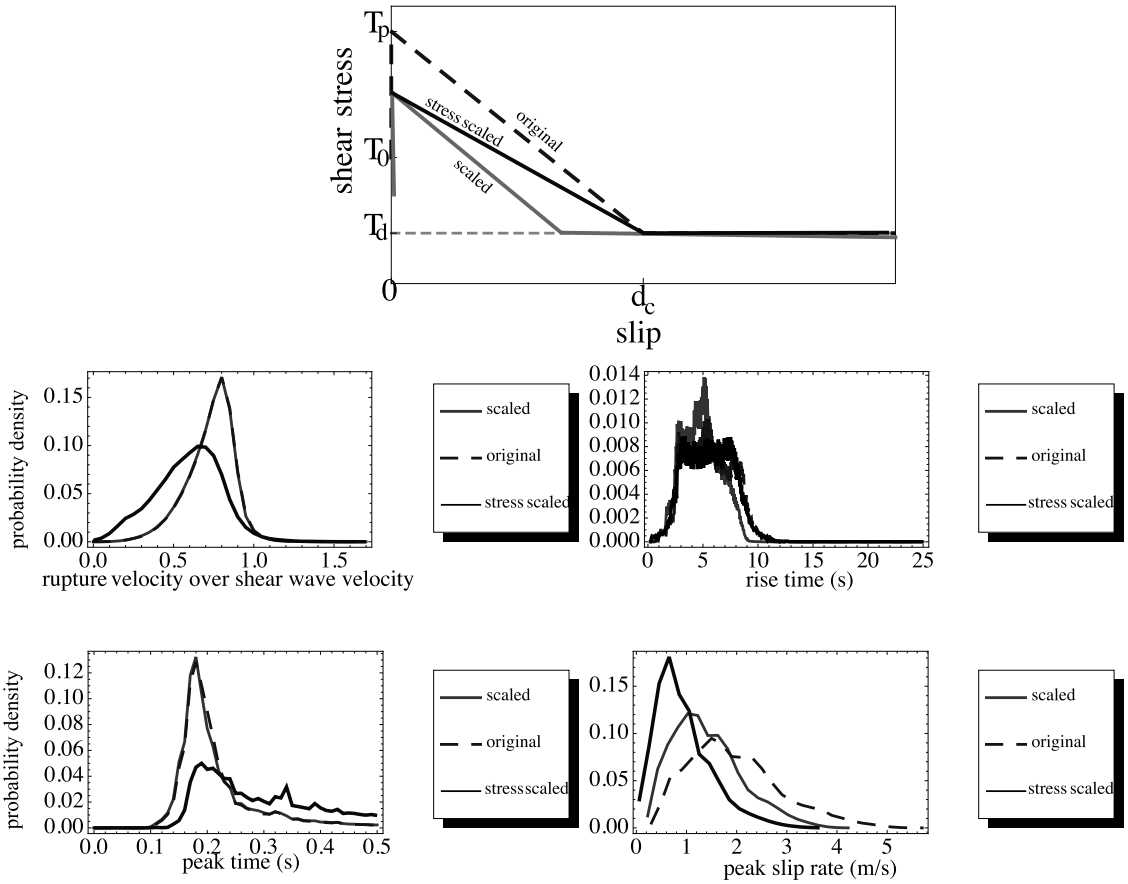

Figure 10. (top) Illustration of slip-weakening law used to rescale models of 6 selected ruptures. "Original" is set 1 (dashed), "scaled" is set 2 (light gray), and "stress scaled" is set 3 (black). (bottom) Comparison of probability density distributions of various source parameters. Even though set 2 (light gray) only has two thirds of the fracture energy of set 1 (dashed), they have the same rupture velocity distribution. Furthermore, set 3 (black) ruptures slower than set 1 (dashed) even though it has smaller fracture energy. This illustrates that the fracture energy is not the single controlling factor for the rupture velocity. The slope of the slip-weakening curve is important as well.

length increases. However, in both the 2-D and 3-D heterogeneous cases, the rupture accelerates, on average, as it propagates away from the hypocenter.

4.6. Outlook

[45] Following the framework of *Liu et al.* [2006], our results suggest that a kinematic rupture model can be constructed using four parameters: s_{kin}, T_p, T_r, and γ. Note that *Liu et al.* [2006] only used slip, risetime, and secant velocity. In their model, the duration of the acceleration phase is computed using CT_r, where C is a constant.

[46] One could utilize the computed correlations and create correlated stochastic fields by assuming the following chain: the slip controls the risetime, the risetime controls the

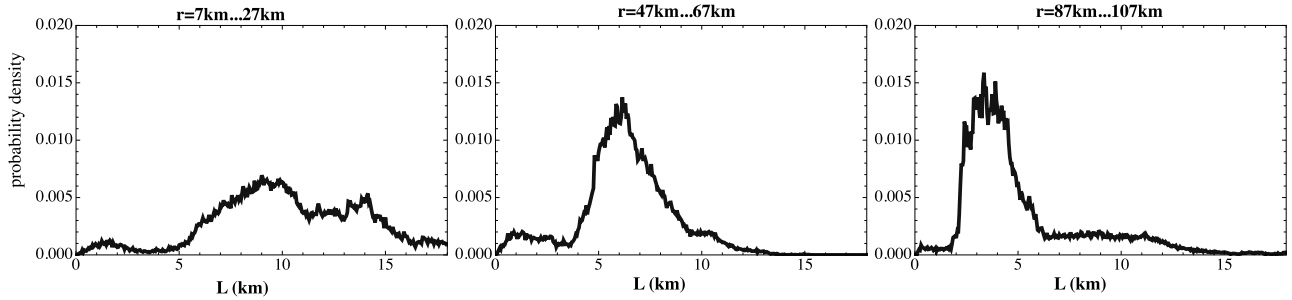

Figure 11. Crack length L as a function of distance. Time weakening computed with 120 km long ruptures [*Andrews*, 2004] were used to compute the probability densities. The crack length decreases as the rupture propagates away from the nucleation zone.

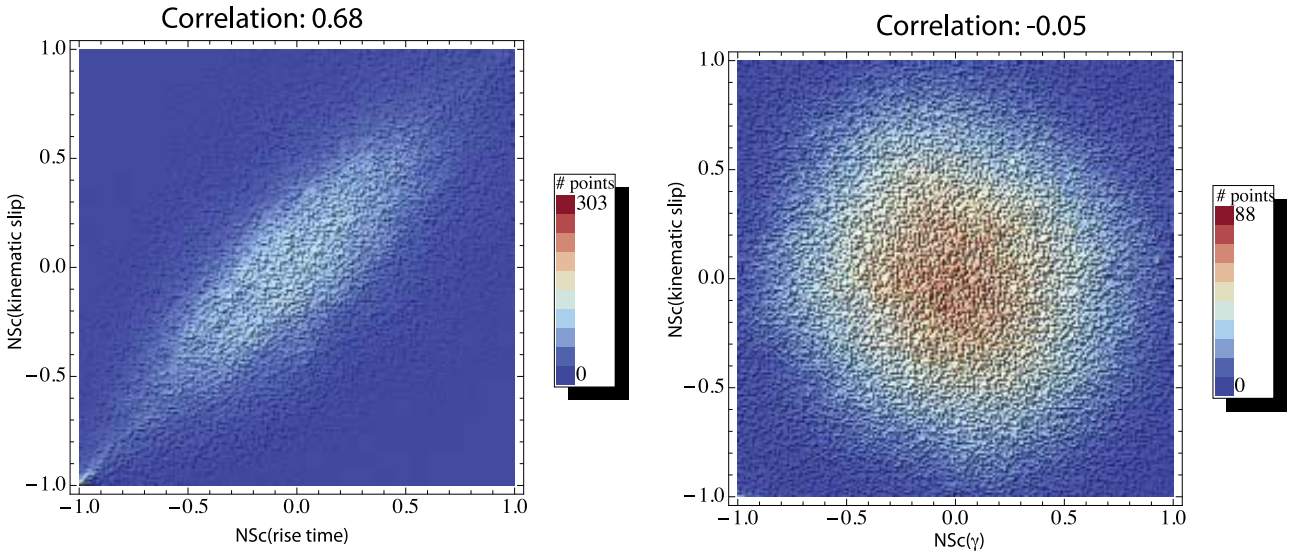

Figure 12. Joint distributions of normal score (NSc) transformed fields computed using 4000 points randomly selected from each rupture. (left) The spatial relation of NSc (slip) and NSc (risetime). A clear positive trend can be found that is reflected in the computed correlation of 0.68. (right) The relation of NSc (slip) and NSc (rupture velocity), which clearly shows no correlation.

peak time, and finally, the peak time controls the rupture velocity. Alternatively, one could also model directly the joint probability distribution of the four parameters. One possible way of doing this is to perform a normal score transform of the parameters. The kth largest value in distribution A gets assigned the kth largest value of a Gaussian random field. This Gaussian field is computed using a normal distribution with mean zero and standard deviation 1 truncated between $[-1, 1]$. Figure 12 plots the joint distribution for slip and rupture velocity and the joint distribution for slip and risetime after the normal score transform. Here it is very clear that no correlation exists between slip and rupture velocity, while slip and risetime correlate well. In the next step, the covariance matrix for the normal score transformed fields is computed and used to construct a multidimensional Gauss distribution. We used all ruptures to compute this covariance matrix, which is plotted in Figure S9.

[47] This multidimensional Gauss distribution can be used to create correlated normal distributed random fields that have the correlation structure of our normal score transformed parameter fields. Then, using the same approach as outlined by *Liu et al.* [2006], one can filter those fields in the wave number domain to achieve spatial coherence. Finally, one transforms each field to the appropriate amplitude distribution.

5. Conclusion

[48] The main goal of this study is to quantify the spatial interdependency of earthquake source parameters computed using dynamic rupture models. The findings can be implemented in a kinematic rupture model. We computed a suite of 315 dynamic ruptures for different sets of initial models using approaches common in the literature. We used a small grid spacing of 60 m that allows the analysis of the ruptures for frequencies up to 5.0 Hz. We also used dynamic ruptures computed by other researchers [*Dalguer et al.*, 2008; *Olsen et al.*, 2009]. The rationale for this procedure is to account for the epistemic uncertainty and to avoid biases. While a lot can be learned by looking at differences among model sets, the focus of this paper is to find characteristics that are common between all computed ruptures. For application to kinematic modeling, we looked for parameter pairs that had a spatial interdependency (correlation) with a small variability in spite of the epistemic and aleatoric variability included in our sets of initial models.

[49] We found that slip (s_{total} or s_{kin}) is not a good control variable for rupture velocity (Figures 4 and S4); its correlation with γ is basically zero. Rupture velocity cannot be expressed as a function of total slip amplitude. This is an important result because such a correlation is often assumed. This assumption can lead to an overprediction of peak ground velocity and peak ground acceleration.

[50] Slip amplitude correlates well with risetime, and risetime correlates well with peak time (T_p), which is related to the time during which the slip rate rises to its maximum. Finally, peak time correlates negatively with normalized rupture velocity (γ). We also found that normalized rupture velocity correlates positively with peak slip rate, and peak slip rate correlates negatively with peak time (Figure 4). These correlations make sense because γ, peak slip rate, and T_p happen on short time scales (during breakdown); while slip and risetime, which are strongly correlated, happen on longer time scales that are controlled by the geometry of the fault and healing phases.

[51] We found that the amplitude distributions of the parameters are distance-dependent (Figure 8). The rupture accelerates as it propagates away from the nucleation zone. With distance from the hypocenter the risetime gets shorter, and the peak slip rate gets larger.

[52] We tested several models with the same heterogeneity in stress and strength but different fracture energy and slip-weakening slope (Figure 10). We found that not only the fracture energy but also the slope in the slip-weakening

curve has control over the rupture velocity and peak time in those models. We found that the crack length in 3-D heterogeneous rupture models decreases as the rupture propagates away from the hypocenter.

[53] Finally, we outlined an approach for implementing our results into a kinematic rupture model generator. It is similar to the one proposed by *Liu et al.* [2006], but instead of creating separate normal distributed fields as a starting point, we proposed using a four-dimensional Gauss distribution that is constructed using the covariance matrix of the normal score transformed parameters slip, risetime, peak time, and rupture velocity.

[54] **Acknowledgments.** We thank Luis Dalguer for providing the DynaShake ruptures. We thank Shuo Ma for providing his finite element code. We thank an anonymous reviewer and Elisa Tinti for valuable comments that improved the manuscript. This research was supported by the Southern California Earthquake Center (SCEC) and by UCSB matching funds to SCEC. SCEC is funded by NSF Cooperative Agreement EAR-0529922 and USGS Cooperative Agreement 07HQAG0008. We have also received support through a gift from Pacific Gas and Electric to the Institute for Crustal Studies (ICS). This material is also based upon work supported by the National Science Foundation under grant 0738954. This is SCEC contribution 1322. This is ICS contribution 1008.

References

Andrews, D. J. (1976a), Rupture propagation with finite stress in antiplane strain, *J. Geophys. Res.*, *81*(20), 3575–3582, doi:10.1029/JB081i020p03575.

Andrews, D. J. (1976b), Rupture velocity of plane strain shear cracks, *J. Geophys. Res.*, *81*(32), 5679–5687, doi:10.1029/JB081i032p05679.

Andrews, D. J. (1980), A stochastic fault model: 1. Static case, *J. Geophys. Res.*, *85*(B7), 3867–3877, doi:10.1029/JB085iB07p03867.

Andrews, D. J. (2004), Rupture models with dynamically determined breakdown displacement, *Bull. Seismol. Soc. Am.*, *94*(3), 769–775, doi:10.1785/0120030142.

Archuleta, R. J. (1984), A faulting model for the 1979 Imperial Valley earthquake, *J. Geophys. Res.*, *89*(B6), 4559–4585, doi:10.1029/JB089iB06p04559.

Campillo, M., P. Favreau, I. R. Ionescu, and C. Voisin (2001), On the effective friction law of a heterogeneous fault, *J. Geophys. Res.*, *106*(B8), 16,307–16,322, doi:10.1029/2000JB900467.

Dalguer, L. A., S. M. Day, K. B. Olsen, and V. M. Cruz-Atienza (2008), Rupture models and ground motion for shakeout and other southern San Andreas fault scenarios, paper presented at 14th World Conference on Earthquake Engineering, Int. Assoc. for Earthquake Eng., Beijing, 12–17 Oct.

Das, S., and K. Aki (1977), A numerical study of two-dimensional spontaneous rupture propagation, *Geophys. J. R. Astron. Soc.*, *50*(3), 643–668.

Day, S. M. (1982), Three-dimensional simulation of spontaneous rupture: The effect of nonuniform prestress, *Bull. Seismol. Soc. Am.*, *72*(6A), 1881–1902.

Eshelby, J. D. (1969), The elastic field of a crack extending non-uniformly under general anti-plane loading, *J. Mech. Phys. Solids*, *17*, 177–199, doi:10.1016/0022-5096(69)90032-5.

Gonzalez, R. C., and R. E. Woods (2002), *Digital Image Processing*, 2nd ed., Prentice Hall, Upper Saddle River, N. J.

Guatteri, M., P. M. Mai, and G. C. Beroza (2004), A pseudo-dynamic approximation to dynamic rupture models for strong ground motion prediction, *Bull. Seismol. Soc. Am.*, *94*(6), 2051–2063, doi:10.1785/0120040037.

Ida, Y. (1972), Cohesive force across the tip of a longitudinal-shear crack and Griffith's specific surface energy, *J. Geophys. Res.*, *77*(20), 3796–3805, doi:10.1029/JB077i020p03796.

Lavallée, D. (2008), On the random nature of earthquake sources and ground motions: A unified theory, in *Earth Heterogeneity and Scattering Effects in Seismic Waves*, *Adv. Geophys.*, vol. 50, edited by H. Sato et al., pp. 427–461Elsevier, New York.

Lavallée, D., P. Liu, and R. J. Archuleta (2006), Stochastic model of heterogeneity in earthquake slip spatial distributions, *Geophys. J. Int.*, *165*(2), 622–640, doi:10.1111/j.1365-246X.2006.02943.x.

Liu, P., R. J. Archuleta, and S. H. Hartell (2006), Prediction of broadband ground-motion time histories: Hybrid low/high- frequency method with correlated random source parameters, *Bull. Seismol. Soc. Am.*, *96*(6), 2118–2130, doi:10.1785/0120060036.

Liu, Y., and N. Lapusta (2008), Transition of mode II cracks from sub-Rayleigh to intersonic speeds in the presence of favorable heterogeneity, *J. Mech. Phys. Solids*, *56*, 25–50, doi:10.1016/j.jmps.2007.06.005.

Ma, S., and P. Liu (2006), Modeling of the perfectly matched layer absorbing boundaries and intrinsic attenuation in explicit finite-element methods, *Bull. Seismol. Soc. Am.*, *96*(5), 1779–1794, doi:10.1785/0120050219.

Ma, S., S. Custódio, R. J. Archuleta, and P. Liu (2008), Dynamic modeling of the 2004 M_w 6.0 Parkfield, California, earthquake, *J. Geophys. Res.*, *113*, B02301, doi:10.1029/2007JB005216.

Mai, P. M., and G. C. Beroza (2002), A spatial random field model to characterize complexity in earthquake slip, *J. Geophys. Res.*, *107*(B11), 2308, doi:10.1029/2001JB000588.

Nelder, J. A., and R. Mead (1965), A simplex method for function minimization, *Comput. J.*, *7*, 308–313.

Nielsen, S., and R. Madariaga (2003), On the self-healing fracture mode, *Bull. Seismol. Soc. Am.*, *93*(6), 2375–2388, doi:10.1785/0120020090.

Oglesby, D. D., and S. M. Day (2002), Stochastic fault stress: Implications for fault dynamics and ground motion, *Bull. Seismol. Soc. Am.*, *92*(8), 3006–3021, doi:10.1785/0120010249.

Olsen, K. B., et al. (2009), ShakeOut-D: Ground motion estimates using an ensemble of large earthquakes on the southern San Andreas fault with spontaneous rupture propagation, *Geophys. Res. Lett.*, *36*, L04303, doi:10.1029/2008GL036832.

Press, W. H., S. A. Teukolsky, W. T. Vetterling, and B. P. Flannery (1992), *Numerical Recipes in C: The Art of Scientific Computing*, 2nd ed., Cambridge Univ. Press, New York.

Ripperger, J., P. M. Mai, and J. P. Ampuero (2008), Variability of near-field ground motion from dynamic earthquake rupture simulations, *Bull. Seismol. Soc. Am.*, *98*(3), 1207–1228, doi:10.1785/0120070076.

Schmedes, J., R. J. Archuleta, and D. Lavallée (2009), Dependency of supershear transition in dynamic rupture simulations on the autocorrelation of initial stress, *Seismol. Res. Lett.*, *80*(2), 301.

Somerville, P., K. Irikura, R. Graves, S. Sawada, D. Wald, N. A. Abrahamson, Y. Iwasaki, N. Smith, and A. Kowada (1999), Characterizing crustal earthquake slip models for the prediction of strong ground motion, *Seismol. Res. Lett.*, *70*, 59–80.

Song, S. G., A. Pitarka, and P. Somerville (2009), Exploring spatial coherence between earthquake source parameters, *Bull. Seismol. Soc. Am.*, *99*(4), 2564–2571, doi:10.1785/0120080197.

Tinti, E., E. Fukuyama, A. Piatanesi, and M. Cocco (2005), A kinematic source-time function compatible with earthquake dynamics, *Bull. Seismol. Soc. Am.*, *95*(4), 1211–1223, doi:10.1785/0120040177.

Tinti, E., M. Cocco, E. Fukuyama, and A. Piatanesi (2009), Dependence of slip weakening distance (D_c) on final slip during dynamic rupture of earthquakes, *Geophys. J. Int.*, *177*(3), 1205–1220, doi:10.1111/j.1365-246X.2009.04143.x.

R. J. Archuleta and J. Schmedes, Department of Earth Science, University of California, Santa Barbara, 1006 Webb Hall, Santa Barbara, CA 93106, USA. (jasch@crustal.ucsb.edu)

D. Lavallée, Institute for Crustal Studies, University of California, 1140 Girvetz Hall, Santa Barbara, CA 93106, USA.